Science Advances
AAAS

Supplementary Materials for

Intermediates in SARS-CoV-2 spike–mediated cell entry

Tara C. Marcink *et al.*

Corresponding author: Tom Gallagher, tgallag@luc.edu; Amédée des Georges, adesgeorges@gc.cuny.edu; Matteo Porotto, mp3509@cumc.columbia.edu; Anne Moscona, am939@cumc.columbia.edu

Sci. Adv. **8**, eabo3153 (2022)
DOI: 10.1126/sciadv.abo3153

The PDF file includes:

Figs. S1 to S8
Legends for movies S1 to S3

Other Supplementary Material for this manuscript includes the following:

Movies S1 to S3

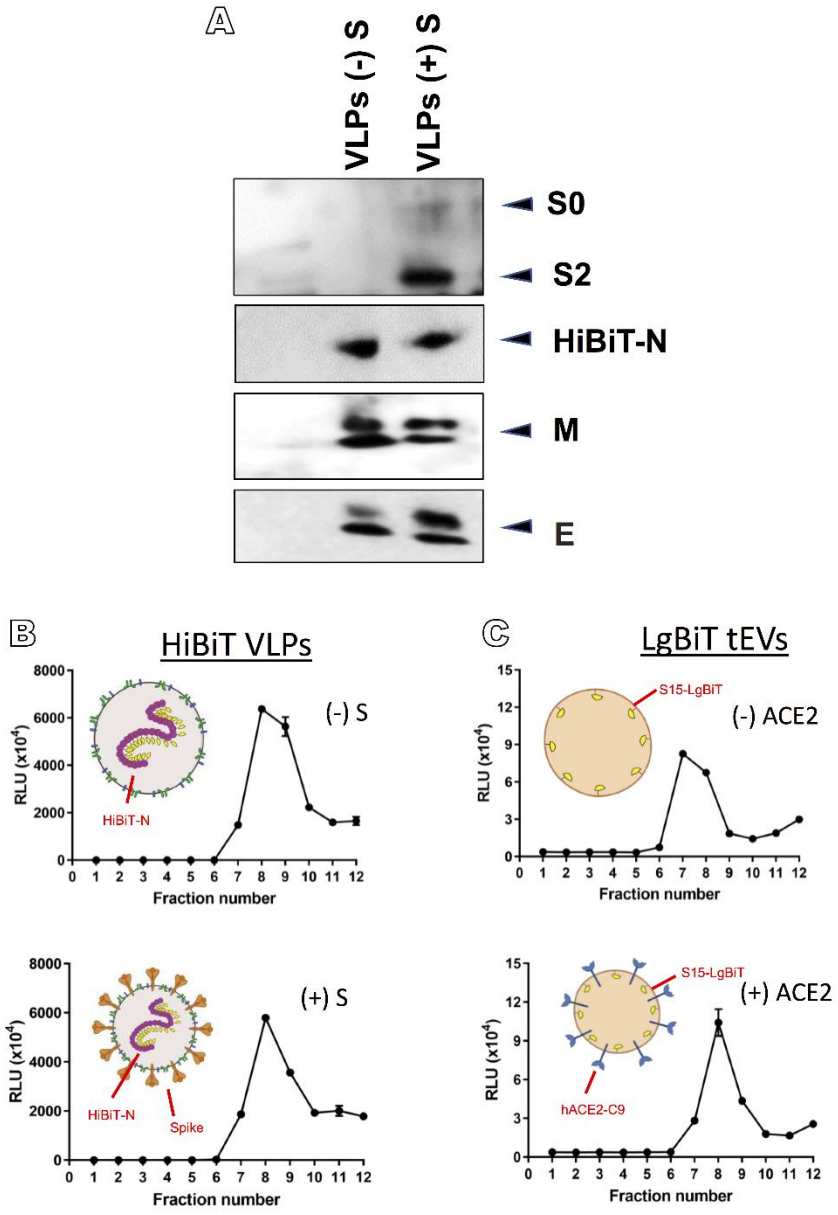

Fig. S1.

Size exclusion chromatographic elution profiles for VLPs and tEVs. (A) Harvested VLPs were electrophoresed, transferred to membranes and probed for the indicated SARS-CoV-2 structural proteins. The resulting immunoblot images reveal the three central CoV structural proteins N, M and E. S0: uncleaved S. S2: Complete S2 without activation to S2'. (B) Concentrated VLPs eluted from IZON qEV SEC columns were detergent-solubilized and detected by complementation with LgBiT and subsequent luminometry. VLP yields (fractions 7-9) were similar regardless of S protein presence. (C) Concentrated tEVs containing membrane-bound S15 LgBiT, eluted from SEC columns, were detergent-solubilized and detected by

complementation with HiBiT-N and subsequent luminometry. tEV yields (fractions 7-9) were similar regardless of ACE2 protein presence. These preparations were used for the experimental results shown in Fig. S2.

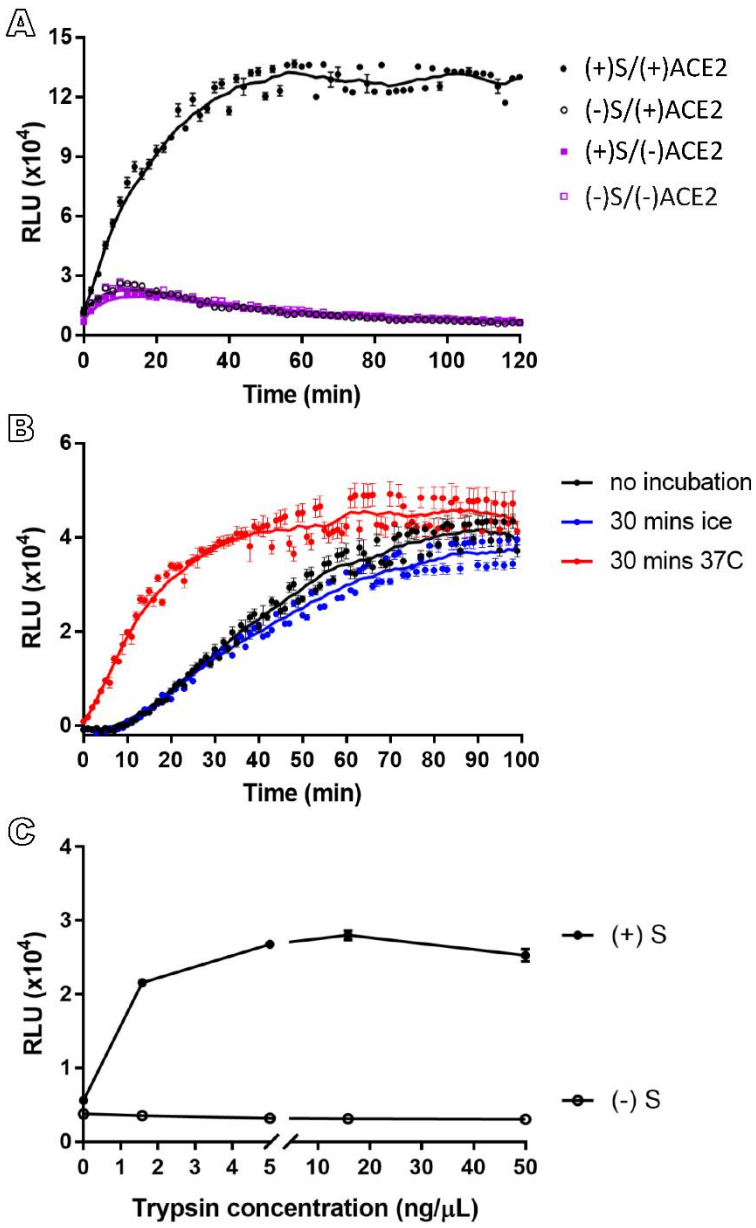

Fig. S2.

Kinetics of VLP / tEV fusion and requirements for S and ACE2. (A) VLPs, with or without S, and tEVs, with or without ACE2, were incubated for 30 min at 37°C. Trypsin and nanoluciferase substrate were added at t = 0 and RLUs were then measured thereafter at 37°C. RLU profiles over time were fit to LOWESS curves using GraphPad Prism software. Fusion signals, measured as development of RLU, required S on VLPs and ACE2 on tEVs. (B) S-positive VLPs were mixed with ACE2-positive tEVs. Trypsin and nanoluciferase substrate were added either with or without pre-incubation of the VLP-tEVs at 37°C, and RLU developments

over time were fit to LOWESS curves using GraphPad Prism software. Fusion kinetics were accelerated by the 37°C pre-incubation. (C) S-positive or S-negative VLPs were mixed on ice with ACE2-positive tEVs in the presence of nanoluciferase substrate. The indicated amounts of trypsin were added, and after 30 min at 37°C, RLU values were determined. Error bars represent standard errors of the mean values (n=3).

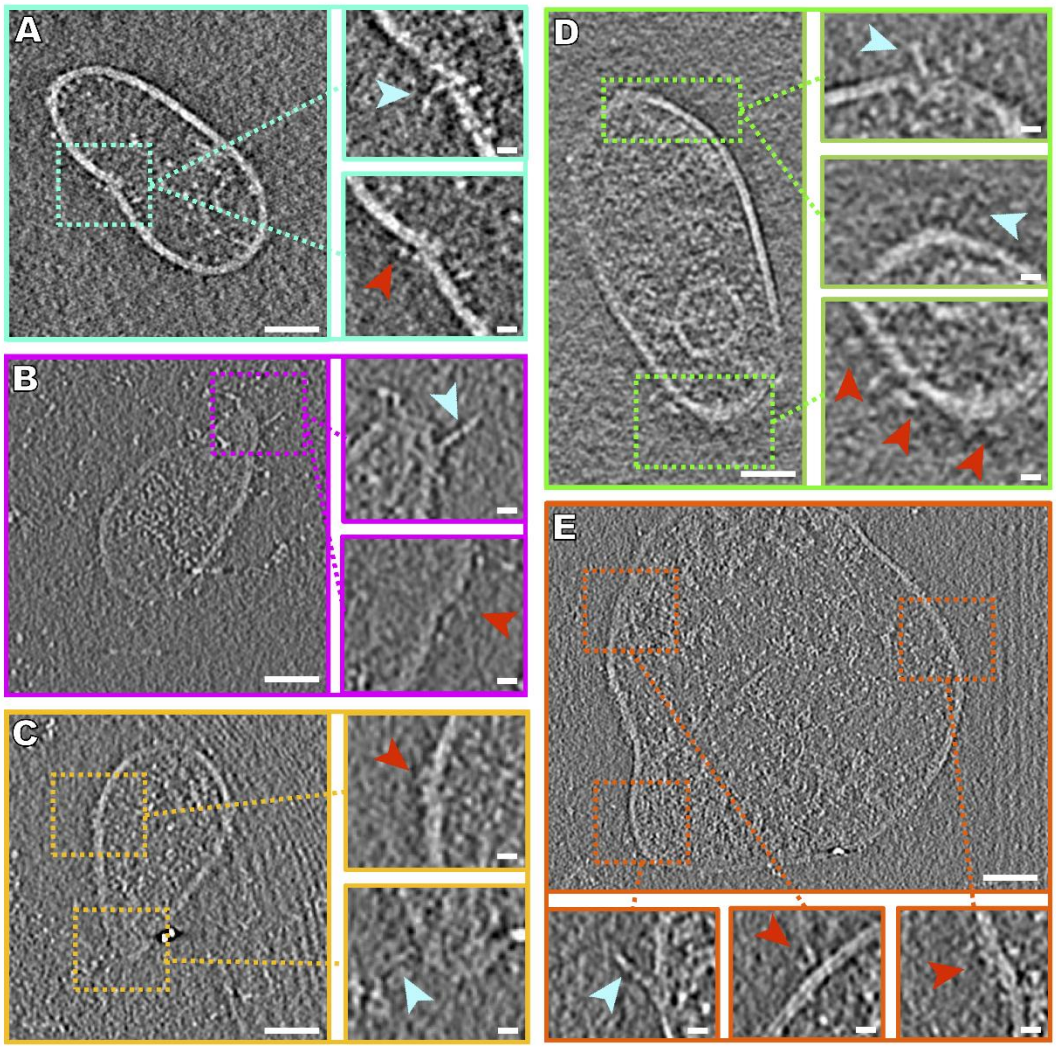

Fig. S3.

Fusion of SARS-CoV-2 VLPs with hACE2 tEVs. (A-E) Contrast-inverted slices through tomogram of VLPs and tEVs that proceeded to full fusion. Densities attributed to hACE2 (red arrows) and spike (cyan arrows) were on the same vesicular membranes. Scale bars: (A-E) 50nm; insets 10 nm.

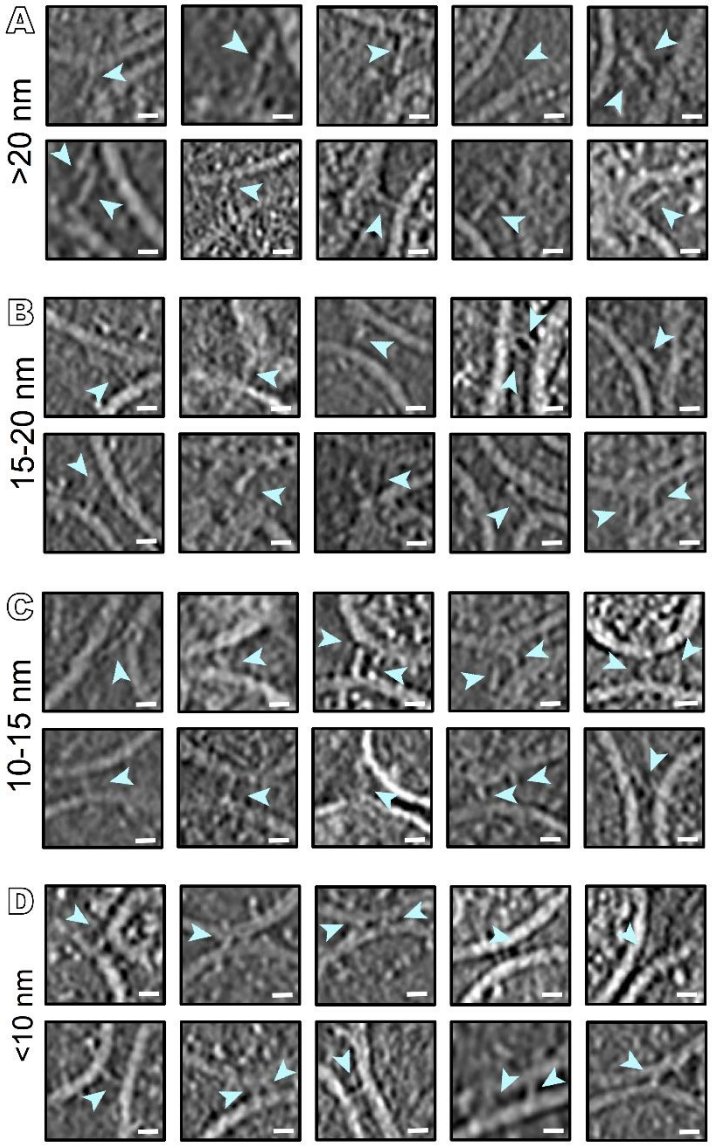

Fig. S4.

Instances of spike intermediates observed at each of 4 intermembrane distance groupings.

Contrast-inverted slices through tomograms from samples containing VLPs, tEVs, trypsin and $[SARS_{HRC}\text{-}PEG_4]_2$-chol lipopeptide. Densities corresponding to spike proteins that spanned the tEV and VLP membranes were grouped into 4 intermembrane distance groupings consisting of (A) over 20 nm; (B) 15-20 nm; (C) 10-15 nm; and (D) below 10 nm between VLP and tEV membranes. Scale bars: (A-D) 10nm

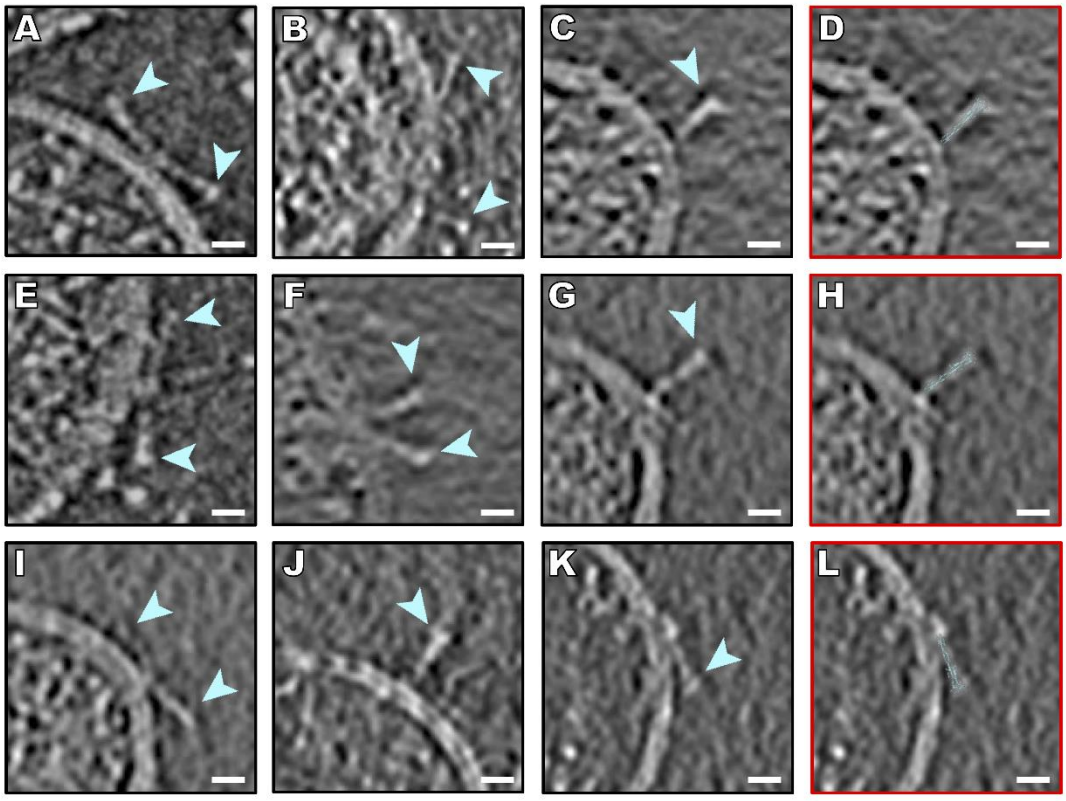

Fig. S5.

Post-fusion spike proteins. (A-I) Contrast-inverted slices through tomograms from samples containing VLPs, tEVs, trypsin and [$SARS_{HRC}$-PEG_4]$_2$-chol lipo-peptide. Densities attributed to spikes distal from the regions of interaction (light blue arrows) are in a post-fusion state. (D,H,L) Tomogram slices from panels C, G, and K with the post-fusion S (light blue) (PDBID:6M3W) fitted into the density. Scale bars: (A-L) 10nm

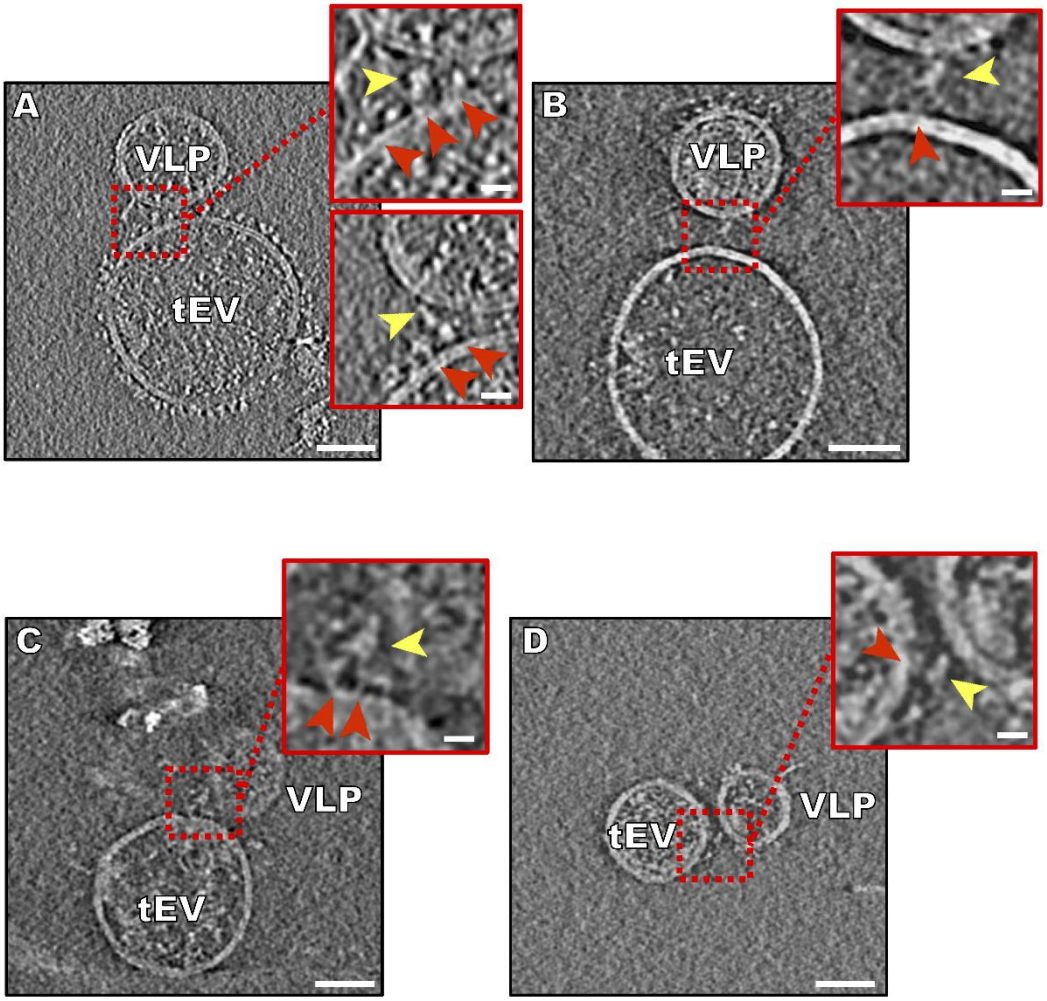

Fig. S6.

Pre-fusion spike-hACE2 interactions at 4°C. (A-D) Tomographic slices through samples incubated at 4°C before vitrification. Densities attributed to pre-fusion spike (yellow arrows) bound to densities attributed to hACE2 (red arrows). Slices through tomograms show interaction between spike and hACE2; insets show enlarged views of these interactions. Spikes can be seen binding multiple hACE2 dimers. Scale bars: (A-D) 50nm; insets 10 nm.

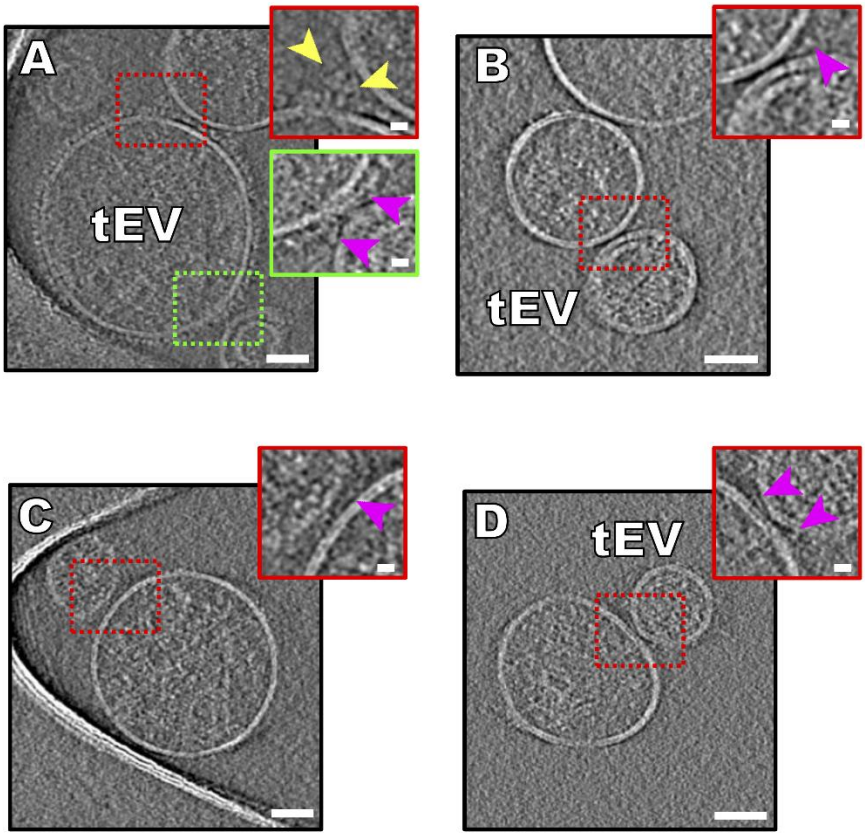

Fig. S7.

Multiple states of the spike protein captured by peptide without lipid moiety. (A-D) Contrast-inverted slices from multiple tomograms where tEVs and VLPs are found in close proximity to each other. Densities attributed to folded intermediates of S2 (purple arrows) and and pre-fusion spikes bound to hACE2 (yellow arrows) were captured with the $[SARS_{HRC}]_2$-PEG_{11} peptide. Scale bars: (A-D) 50nm; insets 10 nm.

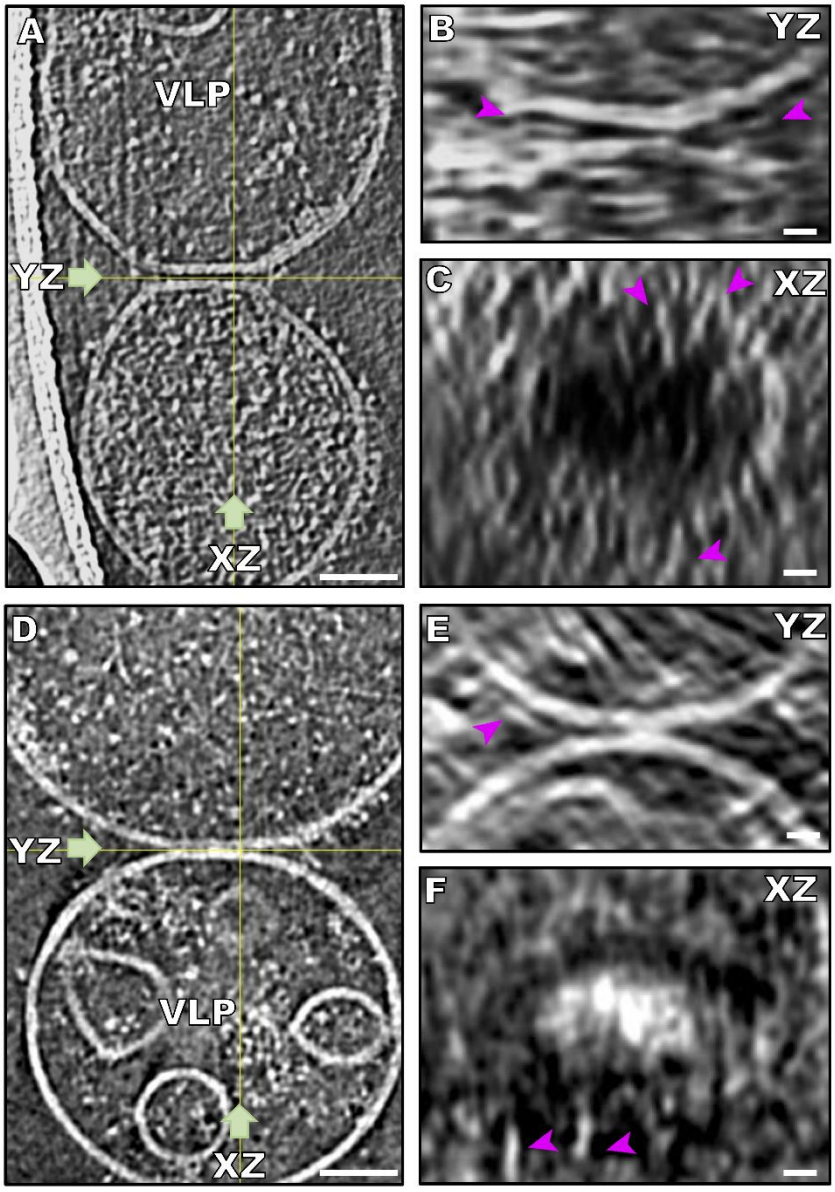

Fig. S8.

Orthogonal projections of VLPs and tEVs in close proximity. (A,D) Contrast-inverted central slices of tomograms with the YZ and XZ directions overlain (yellow lines) from Figure 2 panels 2H and 2K. (B,C,E,F) Orthogonal slices in the YZ (B,E) or XZ (C,F) plane contain densities attributed to folded S2 intermediates spanning the VLP and tEV membranes (purple arrows).

Movie S1.
Tomogram of SARS-CoV-2 spike-bearing virus-like particles (VLPs) interacting with hACE2-bearing extracellular vesicles (tEVs), showing SARS-CoV-2 pre-fusion spike protein in contact with hACE2 (Fig. 3B-E).

Movie S2.
Tomogram of SARS-CoV-2 spike-bearing virus-like particles (VLPs) interacting with hACE2-bearing extracellular vesicles (tEVs), showing various intermediate states of the SARS-CoV-2 spike protein (Fig. 5L,M).

Movie S3.
Tomogram of SARS-CoV-2 spike-bearing virus-like particles (VLPs) interacting with hACE2-bearing extracellular vesicles (tEVs), showing various intermediate states of the SARS-CoV-2 spike protein (Fig. 5N,O and Fig 4J).